Aalto University

OPEN ACCESS

This is an electronic reprint of the original article.
This reprint may differ from the original in pagination and typographic detail.

Dong, Kai; Vorobyov, Sergiy A.; Yu, Hao; Taleb, Tarik

Beamforming Design for Integrated Sensing, Over-the-Air Computation, and Communication in Internet of Robotic Things

Published in:
IEEE Internet of Things Journal

DOI:
10.1109/JIOT.2024.3433390

Published: 01/01/2024

Document Version
Publisher's PDF, also known as Version of record

Published under the following license:
CC BY-NC-ND

Please cite the original version:
Dong, K., Vorobyov, S. A., Yu, H., & Taleb, T. (2024). Beamforming Design for Integrated Sensing, Over-the-Air Computation, and Communication in Internet of Robotic Things. *IEEE Internet of Things Journal*, *11*(20), 32478-32489. https://doi.org/10.1109/JIOT.2024.3433390

This material is protected by copyright and other intellectual property rights, and duplication or sale of all or part of any of the repository collections is not permitted, except that material may be duplicated by you for your research use or educational purposes in electronic or print form. You must obtain permission for any other use. Electronic or print copies may not be offered, whether for sale or otherwise to anyone who is not an authorised user.

Beamforming Design for Integrated Sensing, Over-the-Air Computation, and Communication in Internet of Robotic Things

Kai Dong, *Member, IEEE*, Sergiy A. Vorobyov, *Fellow, IEEE*, Hao Yu, *Member, IEEE*, and Tarik Taleb, *Senior Member, IEEE*

***Abstract*—The integration of communication and radar systems could enhance the robustness of future communication systems to support advanced application demands, e.g., target sensing, data exchange, and parallel computation. In this article, we investigate the beamforming design for integrated sensing, computing, and communication (ISCC) in the Internet of Robotic Things (IoRT) scenario. Specifically, we assume that each robot uploads its preprocessed sensing information to the access point (AP). Meanwhile, leveraging the additive features of the spatial wireless channels between robots and AP, over-the-air computation (AirComp) through multirobot cooperation could bolster system performance, particularly in tasks like target localization through sensing. To get a full picture of the effects of antenna array structures and beampatterns on the ISCC system, we evaluate the performance by considering the shared and separated antenna structures, as well as the omnidirectional and directional beampatterns. Based on these setups, the nonconvex optimization problems for the performance tradeoff between sensing and AirComp are formulated to minimize the mean-squared error (MSE) of AirComp and sensing. To efficiently solve these optimization problems, we designed the gradient descent augmented Lagrangian (GDAL) algorithm, which involves dynamically adjusting the step sizes while updating the variables. Simulation results show that the separated antenna structure achieves a lower AirComp MSE than the shared antenna setup because it has greater beam steering Degrees of Freedom. Moreover, the beampattern types have almost no effect on the AirComp MSE for the given antenna structure setup. This comprehensive investigation provides useful guidelines for ISCC framework implementation in IoRT applications.**

***Index Terms*—Beamforming, integrated sensing, computing, and communication (ISCC), Internet of Robotic Things (IoRT), over-the-air computation (AirComp).**

Manuscript received 22 April 2024; revised 17 June 2024; accepted 14 July 2024. Date of publication 14 August 2024; date of current version 9 October 2024. This work was supported in part by the European Union's HE Research and Innovation Program HORIZON-JUSNS-2023 through the 6G-Path Project under Grant 101139172, and in part by the Business Finland 6Bridge 6Core Project under Grant 8410/31/2022. *(Corresponding author: Hao Yu.)*

Kai Dong is with the Center of Wireless Communications, University of Oulu, 90570 Oulu, Finland (e-mail: kai.dong@oulu.fi).

Sergiy A. Vorobyov is with the Department of Information and Communications Engineering, Aalto University, 02150 Espoo, Finland (e-mail: sergiy.vorobyov@aalto.fi).

Hao Yu is with the Department of Communications and Networking, ICTFicial OY, 02130 Espoo, Finland (e-mail: hao.yu@ictficial.com).

Tarik Taleb is with the Faculty of Electrical Engineering and Information Technology, Ruhr University Bochum, 44801 Bochum, Germany (e-mail: tarik.taleb@rub.de).

Digital Object Identifier 10.1109/JIOT.2024.3433390

I. Introduction

THE EVOLVING wireless technology has been regarded as a pivotal facilitator for the future Internet of Robotic Things (IoRT), a specific use case of the Internet of Things (IoT) ecosystem, owing to its enhanced functionalities in connectivity, communication, and interaction [1]. A smart IoRT system allows robots to exchange information with other robots or an access point (AP) via communication links while simultaneously processing environmental perceptions [i.e., integrated sensing and communication (ISAC)] to meet various Quality-of-Service (QoS) requirements, such as accurate target localization and low-latency communications [2], [3], [4]. In such a system, continuous sensing (e.g., radar sensing) by each robot for target detection or tracking collects vast amounts of data, posing new challenges for timely data processing. To address these challenges, designing an efficient integrated sensing, computing, and communication (ISCC) framework tailored to meet the demanding QoS requirements in IoRT is of paramount importance.

The ISCC is crucial for IoRT systems to achieve real-time decision making, efficient resource utilization, and robust fault tolerance.

1) *Real-Time Decision Making:* The IoRT system operates in dynamic and uncertain environments where quick decision making is required. In the ISCC system framework, the robots can collect real-time data from their surroundings via sensing (e.g., radar), process it locally or collaboratively, and make autonomous decisions without relying solely on a centralized controller or human intervention [5].
2) *Enhanced Resource Utilization Efficiency:* Integrated IoRT systems can enhance resource utilization efficiency by leveraging distributed sensing and computation. Specifically, instead of transmitting raw sensor data to a central processing unit (e.g., an edge server), robots can preprocess and analyze data locally to reduce data transmission and further minimize latency. Moreover, both radar sensing and data transmission using the same spectrum and signals can improve spectral and energy efficiencies, making IoRT systems more efficient and scalable for simultaneously serving multiple robots [6].
3) *Robust Error-Fault Tolerance:* The IoRT system enables robots to collaborate with each other to achieve common

© 2024 The Authors. This work is licensed under a Creative Commons Attribution-NonCommercial-NoDerivatives 4.0 License. For more information, see https://creativecommons.org/licenses/by-nc-nd/4.0/

goals or tasks. For example, when multiple robots send their collected sensing information about one common target to the edge server via multiaccess wireless channels, the localization parameter estimation leveraging the information from multiple robots could achieve an enhanced robustness for errors (faults) compared to a single robot [7].

The dual-functional waveform design has been widely investigated in radar-communication systems [8], [9], [10], [11], [12], [13], [14]. The optimal waveform design with constraint of a fixed transmit power, for achieving the sensing and downlink communication performance tradeoff has been investigated in [11] where the radar system was mounted at the base station (BS). By fully using the waiting time in conventional pulsed radar to transmit dedicated communication signals, the waveform has been designed to improve the communication spectrum efficiency and probability of target detection in a full-duplex ISAC scheme [13]. From the perspective of information theory [mutual information (MI)], another waveform has been designed to maximize the sensing and communication MI [14]. To detect the target behind the obstacle, the reconfigurable intelligent surface (RIS) has also been utilized to assist the downlink simultaneous target sensing and communication via beamforming design [15]. In [16], unmanned aerial vehicles (UAVs) have been designed to provide ISAC services for multiple IoT nodes to maximize the minimum data rate. Although the aforementioned works focus on ISAC waveform design to enhance system performance, they all consider a shared antenna setup for dual-functional radar-communication waveform radiation. The alternative separated antenna configuration, where communication and sensing use different antenna arrays on the robot, is often overlooked. This approach has been shown to improve the Degrees of Freedom (DoFs) for beam steering in both communication and sensing [17]. Moreover, the relevant processing schemes for data collected during the sensing stage were not included in the ISAC system evaluation.

In mobile IoRT systems, the robots need to continuously perform sensing for environment perception, object detection (e.g., obstacles and landmarks), and localization [2]. There will be enormous amounts of raw data collected at the sensors. Therefore, related data processing (computation) scheme is necessary. However, the limited battery capacity of mobile robots necessitates the design of energy-efficient computation schemes. Currently, the binary computation task offloading scheme for data processing has been widely investigated [18], [19], [20], [21], [22], [23]. In this scheme, computation tasks are executed either locally at the user, remotely at the AP, or at another user device with computation capabilities [22]. The computation results are then fed back to the user via communication links. Additionally, a new computation paradigm called air computation (AirComp), which fully utilizes the additive properties of analog signals via multiaccess wireless channels through multi-IoT device cooperation, has been proposed as a promising method for fast data aggregation at a centralized receiver (e.g., BS or AP) or for distributed computations in the physical layer [24], [25], [26], [27], [28]. This approach eliminates the need for additional computation operations at the receiver side. In the IoRT system, limited observation of the target or false detection due to blockages between the robot and target can affect target detection accuracy at a single robot. Alternatively, target localization accuracy can be improved using the AirComp scheme, where multiple robots cooperatively send their locally computed estimates of target parameters to the AP. In such a scheme, the parameter estimation accuracy for the common target only needs to be approximately correct, and the use of AirComp in a distributed IoRT system enhances the overall estimation accuracy [28]. The final computation result is then broadcast to the robots via downlink communications, reducing the computational burden and prolonging battery life at each robot, thereby improving accurate target localization. Therefore, the integration of AirComp with ISAC technology, i.e., the ISCC framework, has many advantages, such as improved spectrum efficiency using the same spectrum resources and enhanced system performance (e.g., target localization) through multidevice cooperation [6], [25], [29], [30], [31]. In [6], the radar and communication signals transmitted through shared or separated antenna arrays have been considered for wireless sensor networks. The beamforming design has been optimized to minimize AirComp errors. The beampattern has been designed in [32] to achieve a performance tradeoff between sensing and AirComp constrained by the power budget at each device. In particular, omnidirectional and directional beampatterns were considered. Similarly, the performance tradeoff among communication, sensing, and computation under power constraints has been investigated in [30]. Qi et al. [25] designed beamforming for sending a superposition-coded signal to the BS over the uplink channel for computation and communication. The minimum communication data rate and power constraints have been considered when determining the optimal beamforming matrix. However, the aforementioned literature does not have a comprehensive analysis of the antenna array structures (shared or separated) and the beampatterns (omnidirectional or directional). Furthermore, these works evaluate the system performance using a random Gaussian channel realization rather than considering practical path loss in high-frequency bands or link conditions such as blockage. Those realistic setups will be considered in this article in the IoRT scenario, as depicted in Fig. 1.

The specific contributions of this article are as follows.

1) In addition to the shared and separated antenna array structures at each robot for both communication and sensing, we also take into account the omnidirectional and directional beampatterns to conduct a comprehensive comparison between these near-realistic setups in an IoRT scenario.
2) To achieve a performance tradeoff between sensing and AirComp, several nonconvex mean-squared error (MSE) minimization-based optimization problems are formulated under the constraints of maximum transmit power and sensing QoS requirements for different antenna array setups and beampatterns.
3) To solve these nonconvex optimization problems efficiently, we designed a gradient descent augmented Lagrangian (GDAL) algorithm with adaptive adjustment

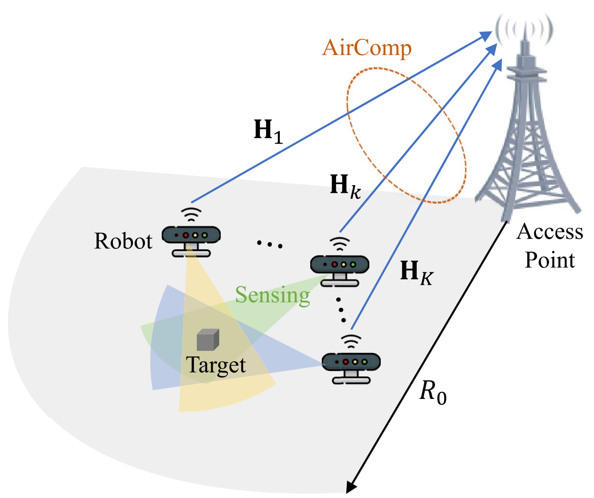

Fig. 1. ISCC framework implemented in an IoRT scenario.

of the step size when updating the variable using gradient descent method.

4) The propagation of electromagnetic wave signals between the robot and AP is prone to being blocked in the high-frequency bands. Here, we also explore the AirComp MSE affected by the robot–AP link blockage that happened with a certain probability.

The remainder of this article is organized as follows. Section II introduces the system models for two different antenna structures at robots. The optimal beampattern design for radar sensing is described in Section III. Section IV introduces the optimization problem and gives corresponding algorithm for the performance tradeoff optimization between sensing and AirComp. Numerical simulation results and conclusion remarks are presented in Sections V and VI, respectively.

Notations: In this article, we use bold lowercase letters (e.g., $\mathbf{a}$) and bold uppercase letters (e.g., $\mathbf{A}$) to represent vectors and matrices, respectively. By normal fonts (e.g., a), we denote the scalars. Moreover, $\mathbf{Tr}(\cdot)$ stands for the trace operation, $(\cdot)^H$ denotes the Hermitian transpose operation, $\|\cdot\|_F$ represents the Frobenius norm of a matrix, $|\cdot|$ is the absolute value, and $\mathbf{I}$ is the identity matrix.

II. System Model

Consider a scenario with K robots randomly distributed at the sector coverage area of an AP with a radius of R_0, as illustrated in Fig. 1. There is a common point-like static target located at $[x_0, y_0]$. Accurate parameter estimation (e.g., coordinates and angle) of the target becomes of paramount importance for safety operation at the robot itself, or for end-to-end wireless link quality guarantees for the robot through proper propagation path scheduling. In this IoRT scenario with an ISCC framework, each robot simultaneously transmits the signals for target sensing and data transmission to the AP for AirComp. Assuming that the data symbols sent from each robot to the AP convey the estimated position information about the target in the last time slot, the AirComp using multirobot cooperation could improve the target localization accuracy [6]. This is crucial for centralized resource management on the whole IoRT scenario.

The robots and AP are assumed to be equipped with uniform linear arrays (ULAs) of N_R and N_A antenna elements, respectively. In particular, the N_t antenna elements out of the N_R ones at each robot are used for signal transmission, and the other $N_r = N_R - N_t$ ones are used for signal reception. The channel between the AP and each robot $k \in \mathcal{K} = \{1, 2, \ldots, K\}$ is assumed to be block-fading and the channel state information (CSI) is assumed to be accurately known at the AP. In mobile robotic networks operating in high-frequency bands, the electromagnetic wave signal propagation between AP and robots is prone to being blocked by the surrounding environment.[1] Here, we assume that the propagation link between AP and each robot is in a Line-of-Sight (LoS) condition with probability $1-p_b$, where $p_b \in [0, 1]$ denotes the blockage probability, and the path loss is calculated according to Third Generation Partnership Project (3GPP) [35].

The received signal model at the AP depends on the antenna configurations of the robots, i.e., the sensing signals and the communication symbols can be either jointly transmitted using one shared transmitting antenna array via a dual-functional waveform or separately sent via two isolated ULAs. Both options will be presented in the following sections.

A. Shared Antenna Configuration

In the shared antenna configuration, all the N_t transmitting antenna elements at each robot are used for both target sensing and data transmission to the AP, and the other N_r antennas are used for signal reception. The data symbols transmitted by the kth robot for AirComp are expressed as $\mathbf{s}_k[t] = \{g_{k,1}(\cdot), g_{k,2}(\cdot), \ldots, g_{k,M}(\cdot)\} \in \mathbb{C}^{M\times 1}$, where M is the number of functions to be computed [25], and $g_{k,m}(\cdot)$ represents the preprocessing function at the kth robot. We assume the transmitted data symbols to be independent and identically distributed (i.i.d.), with zero mean and unit variance, i.e., $\mathbb{E}[\mathbf{s}_k[t]\mathbf{s}_k[t]^H] = \mathbf{I}_M$ and $\mathbb{E}[\mathbf{s}_k[t]\mathbf{s}_\varrho[t]^H] = \mathbf{0}\forall\, k \neq \varrho$. Then, the transmitted signal can be written as

$$\mathbf{x}_k[t] = \mathbf{F}_k\mathbf{s}_k[t] \tag{1}$$

where $\mathbf{F}_k \in \mathbb{C}^{N_t\times M}$ denotes the beamforming precoder implemented at the kth robot. Generally, the signals reflected by the target are vanished at the AP due to the long distance between the robot and AP. Thus, the received signal vector with the beamforming combiner $\mathbf{W} \in \mathbb{C}^{N_A\times M}$ at the AP can be formulated as

$$\mathbf{y}[t] = \sum_{k=1}^{K} \mathbf{W}^H\mathbf{H}_k\mathbf{F}_k\mathbf{s}_k[t] + \mathbf{W}^H\mathbf{n} \tag{2}$$

where $\mathbf{H}_k \in \mathbb{C}^{N_A\times N_t}$ denotes the multiple-input–multiple-output (MIMO) channel between the kth robot and AP, and $\mathbf{n} \in \mathbb{C}^{N_A\times 1}$ is the AWGN noise vector such that $\mathbf{n} \sim \mathcal{CN}(\mathbf{0}, \sigma_n^2\mathbf{I})$. Limited by the power budget $P_{\max}$ for the precoder design at each robot, we should meet the following constraint:

$$\|\mathbf{F}_k\|_F^2 \leq P_{\max}\ \forall k. \tag{3}$$

[1]The blockage effect can be mitigated by emerging relaying technologies, such as smart repeaters and reconfigurable metasurfaces, refer to [33] and [34] for more details.

Assuming that the channel matrix $\mathbf{H}_k$ between AP and each robot is known at the AP,[2] the ideal received signal $\tilde{\mathbf{y}}[t]$ (i.e., no link blockage and with optimal beamforming design) is given by

$$\tilde{\mathbf{y}}[t] = \sqrt{\frac{P_t}{M}} \sum_{k=1}^{K} \mathbf{U}^H \mathbf{H}_k \mathbf{V}_k \mathbf{s}_k[t] \tag{4}$$

where $P_t \le P_{\max}$ denotes the transmit power at the robot for both sensing and AirComp signal transmission via the dual-functional waveform, $\mathbf{V}_k \in \mathbb{C}^{N_t \times M}$ contains the first M right singular vectors in the singular value decomposition (SVD) of $\mathbf{H}_k$, i.e., the optimal beamforming precoders for implementation, $\mathbf{U} \in \mathbb{C}^{N_A \times M}$ collects the first M left singular vectors of the SVD of $\sum_{k=1}^{K} \mathbf{H}_k$, i.e., the designed aggregation beamforming combiner at AP for receiving the signals from all the K robots. Note that the beamforming design steered to the dominant signal reception directions based on SVD of the MIMO channel by exploiting channel sparsity has been widely utilized for maximizing the received signal power [38], [39]. Thereby, we derive the aforementioned optimal precoders at each robot based on the channel between the robot and AP, and the optimal aggregation combiners at AP according to the summation of all the channels between robots and AP. Then, we can get the ideal received signal in (9) and regard it as a benchmark for MSE computation of the received signal (2) as

$$\begin{aligned} \mathbf{MSE}_{\text{AirComp}} &= \mathbb{E}_t\Big[|\mathbf{y}[t] - \tilde{\mathbf{y}}[t]|^2 \Big] \\ &= \sum_{k=1}^{K} \| \mathbf{W}^H \mathbf{H}_k \mathbf{F}_k - \mathbf{A} \|_F^2 + \sigma_n^2 \| \mathbf{W} \|_F^2 \end{aligned} \tag{5}$$

where $\mathbf{A} \triangleq \sqrt{\frac{P_t}{M}} \mathbf{U}^H \mathbf{H}_k \mathbf{V}_k$.

B. Separated Antenna Configuration

Unlike the shared antenna configuration for both sensing and communication via the dual-functional waveform at each robot, the transmitting antennas are split into two sub-ULA arrays ($N_t = N_s + N_c$) in the separated antenna structure. Here, N_s antenna elements are used for radar sensing and N_c antenna elements are used for data transmission to the AP. The sensing symbols at the kth robot can be denoted as $\mathbf{d}_k[t] \in \mathbb{C}^{\bar{M} \times 1}$ where $\bar{M}$ represents the number of beams for radar sensing ($\bar{M} \ge 1$), and $\mathbb{E}[\mathbf{d}_k[t]\mathbf{d}_k[t]^H] = \mathbf{I}_{\bar{M}}$ and $\mathbb{E}[\mathbf{d}_k[t]\mathbf{d}_t[t]^H] = \mathbf{0} \forall k \neq \varrho$. Similar to the shared antenna configuration, the data symbols uploaded to the AP for AirComp are expressed as $\mathbf{s}_k[t] \in \mathbb{C}^{M \times 1}$, where M is the number of functions to be computed. Then, the transmitted signals from each robot can be written as

$$\mathbf{x}_k[t] = \begin{bmatrix} \bar{\mathbf{F}}_k \mathbf{d}_k[t] \\ \mathbf{F}_k \mathbf{s}_k[t] \end{bmatrix} \tag{6}$$

where $\mathbf{F}_k \in \mathbb{C}^{N_c \times M}$ and $\bar{\mathbf{F}}_k \in \mathbb{C}^{N_s \times \bar{M}}$ are the beamformers for data transmission and radar sensing, respectively. Ignoring the signals reflected from the target to the AP, due to the large distance, the received aggregated symbol vector $\mathbf{y}[t]$ at the AP can be expressed as

$$\mathbf{y}[t] = \sum_{k=1}^{K} \big(\mathbf{W}^H \mathbf{H}_k \mathbf{F}_k \mathbf{s}_k[t] + \mathbf{W}^H \bar{\mathbf{H}}_k \bar{\mathbf{F}}_k \mathbf{d}_k[t] \big) + \mathbf{W}^H \mathbf{n} \tag{7}$$

where $\bar{\mathbf{H}}_k \in \mathbb{C}^{N_A \times N_s}$ and $\mathbf{H}_k \in \mathbb{C}^{N_A \times N_c}$ represent the MIMO channels between AP and the kth robot for sensing signals and data transmission, respectively, and $\mathbf{n} \in \mathbb{C}^{N_A \times 1}$ is the i.i.d. noise vector such that $\mathbf{n} \sim \mathcal{CN}(\mathbf{0}, \sigma_n^2 \mathbf{I})$.

Similar to the shared antenna configuration, both designed transmitting precoders $\bar{\mathbf{F}}_k$ and $\mathbf{F}_k$ should meet the maximal transmit power constraint that takes the following form:

$$\|\bar{\mathbf{F}}_k\|_F^2 + \|\mathbf{F}_k\|_F^2 \le P_{\max} \ \forall k. \tag{8}$$

Similar to the signal model of the shared antenna structure, the ideal received signal $\tilde{\mathbf{y}}[t]$ (given the knowledge about channel $\mathbf{H}_k$ between AP and each robot) can be expressed as

$$\tilde{\mathbf{y}}[t] = \sqrt{\frac{P_t}{M}} \sum_{k=1}^{K} \mathbf{U}^H \mathbf{H}_k \mathbf{V}_k \mathbf{s}_k[t] \tag{9}$$

where $P_t \le P_{\max}$ is the transmit power for AirComp, and $\mathbf{V}_k \in \mathbb{C}^{N_s \times M}$ and $\mathbf{U} \in \mathbb{C}^{N_A \times M}$ have the same expressions as in (9).

The corresponding MSE between the received signal (7) and the ideal one $\tilde{\mathbf{y}}[t]$ in (9) is given by

$$\begin{aligned} \mathbf{MSE}_{\text{AirComp}} &= \mathbb{E}_t\Big[|\mathbf{y}[t] - \tilde{\mathbf{y}}[t]|^2 \Big] \\ &= \sum_{k=1}^{K} \| \mathbf{W}^H \mathbf{H}_k \mathbf{F}_k - \mathbf{A} \|_F^2 \\ &\quad + \sum_{k=1}^{K} \| \mathbf{W}^H \bar{\mathbf{H}}_k \bar{\mathbf{F}}_k \|_F^2 + \sigma_n^2 \| \mathbf{W} \|_F^2 . \end{aligned} \tag{10}$$

III. Beampattern Design

According to the knowledge level about the target, the beampattern design can be divided into two types: omnidirectional and directional beampatterns. The former design is suitable for the blinding sensing stage, where there is a lack of knowledge about the target direction. It is the case for example during the initial target sensing stage. On the other hand, the second design is specifically targeted for situations where the sensing directions are known and the target is being tracked. Corresponding beampattern designs are introduced next.

A. Omnidirectional Beampattern Design

For the omnidirectional beampattern, the beamforming matrix $\mathbf{F}_k$ should be orthogonal with an identity covariance matrix [11]. To minimize the AirComp errors defined in (5) and (10), the following optimization problems are formulated for two different antenna configurations that are stated in Section II. For shared antenna configuration

$$\mathbf{P1.1} \quad \min_{\mathbf{F}, \mathbf{W}} \quad \mathcal{F}_{1.1}(\mathbf{F}_k, \mathbf{W}) = \sum_{k=1}^{K} \| \mathbf{W}^H \mathbf{H}_k \mathbf{F}_k - \mathbf{A} \|_F^2 + \sigma_n^2 \| \mathbf{W} \|_F^2 \tag{11a}$$

[2]For related channel estimation methods, refer to [36] and [37].

$$\text{s.t.} \quad \|\mathbf{F}_k\|_F^2 = P_{\max}\ \forall k \tag{11b}$$

and for separated antenna configuration

$$\mathbf{P2.1} \quad \min_{\mathbf{F},\mathbf{W},\bar{\mathbf{F}}} \quad \mathcal{F}_{2.1}\big(\mathbf{F}_k, \mathbf{W}, \bar{\mathbf{F}}_k\big) = \sum_{k=1}^{K}\|\mathbf{W}^H\mathbf{H}_k\mathbf{F}_k - \mathbf{A}\|_F^2 + \sum_{k=1}^{K}\|\mathbf{W}^H\bar{\mathbf{H}}_k\bar{\mathbf{F}}_k\|_F^2 + \sigma_n^2\|\mathbf{W}\|_F^2 \tag{12a}$$

$$\text{s.t.} \quad \|\mathbf{F}_k\|_F^2 + \|\bar{\mathbf{F}}_k\|_F^2 = P_{\max}\forall k. \tag{12b}$$

Note that those two problems are nonconvex due to the quadratic power constraints in (11b) and (12b). Although an alternating optimization (AO) approach can be utilized to solve problem **P1.1** as described in [32], the joint optimization of $\mathbf{F} = \{\mathbf{F}_1, \ldots, \mathbf{F}_k, \ldots, \mathbf{F}_K\}$ and $\bar{\mathbf{F}} = \{\bar{\mathbf{F}}_1, \ldots, \bar{\mathbf{F}}_k, \ldots, \bar{\mathbf{F}}_K\}$ makes it an inefficient approach for solving problem **P2.1**. Here, we design a GDAL algorithm. In particular, the gradient descent approach is utilized to update the desired variables $\mathbf{F}_k, \bar{\mathbf{F}}_k$, and $\mathbf{W}$ based on the augmented Lagrangian function. In the following, the detailed procedures using the proposed GDAL approach for solving problem **P2.1** are presented.[3]

First, the augmented Lagrangian function for problem **P2.1** is defined in (13), shown at the bottom of the page, where λ_k denotes the Lagrange multiplier and ρ represents the penalty parameter. After initializing the required parameters, we calculate the gradients with respect to $\mathbf{F}_k$, $\mathbf{W}$, and $\bar{\mathbf{F}}_k$ at each iteration as follows:

$$\begin{aligned}\nabla_{\mathbf{W}}\mathcal{L}_{P2.1} =\ & 2\sum_{k=1}^{K}\mathbf{H}_k\mathbf{F}_k\big(\mathbf{W}^H\mathbf{H}_k\mathbf{F}_k - \mathbf{A}\big)\\ & + 2\sum_{k=1}^{K}\bar{\mathbf{H}}_k^H\bar{\mathbf{F}}_k\mathbf{W}^H\bar{\mathbf{H}}_k\bar{\mathbf{F}}_k + 2\sigma_n^2\mathbf{W}\end{aligned} \tag{14}$$

$$\begin{aligned}\nabla_{\mathbf{F}_k}\mathcal{L}_{P2.1} =\ & 2\mathbf{H}_k^H\mathbf{W}\big(\mathbf{W}^H\mathbf{H}_k\mathbf{F}_k - \mathbf{A}\big) + 2\lambda_k\mathbf{F}_k\\ & + 2\rho\Big(\|\mathbf{F}_k\|_F^2 + \|\bar{\mathbf{F}}_k\|_F^2 - P_{\max}\Big)\ \forall k\end{aligned} \tag{15}$$

$$\begin{aligned}\nabla_{\bar{\mathbf{F}}_k}\mathcal{L}_{P2.1} =\ & 2\bar{\mathbf{H}}_k^H\mathbf{W}\big(\mathbf{W}^H\bar{\mathbf{H}}_k\bar{\mathbf{F}}_k - \mathbf{A}\big) + 2\lambda_k\bar{\mathbf{F}}_k\\ & + 2\rho\Big(\|\mathbf{F}_k\|_F^2 + \|\bar{\mathbf{F}}_k\|_F^2 - P_{\max}\Big)\ \forall k.\end{aligned} \tag{16}$$

Then, the optimization variables at the lth iteration can be updated as

$$\mathbf{W}^{l+1} = \mathbf{W}^l - \mathbf{\Phi}_{\mathbf{W}}^l\nabla_{\mathbf{W}}\mathcal{L}_{P2.1} \tag{17}$$

$$\mathbf{F}_k^{l+1} = \mathbf{F}_k^l - \mathbf{\Phi}_{\mathbf{F}_k}^l\nabla_{\mathbf{F}_k}\mathcal{L}_{P2.1}\ \forall k \tag{18}$$

$$\bar{\mathbf{F}}_k^{l+1} = \bar{\mathbf{F}}_k^l - \mathbf{\Phi}_{\bar{\mathbf{F}}_k}^l\nabla_{\bar{\mathbf{F}}_k}\mathcal{L}_{P2.1}\ \forall k. \tag{19}$$

[3]The procedure for solving problem **P1.1** follows similar steps, and thus, it is not presented here for the sake of brevity.

Traditional stochastic gradient descent approaches use a global step size for all variables, which is inefficient as it does not account for the scale of the gradients. Alternatively, the step sizes $\mathbf{\Phi}_{\mathbf{W}}^l$, $\mathbf{\Phi}_{\mathbf{F}_k}^l$, and $\mathbf{\Phi}_{\bar{\mathbf{F}}_k}^l$ at the lth iteration can be adaptively updated using the adaptive gradient algorithm (AdaGrad) [40], [41], [42] based on accumulated historical gradients. This approach accelerates the convergence process compared to fixed step size methods. Specifically, parameters with larger gradients will experience a rapid decrease in their effective step size, preventing overshooting and stabilizing the convergence process. Conversely, parameters with smaller accumulated gradients will maintain relatively larger step sizes, speeding up convergence. This strategy is particularly useful in avoiding large and unstable updates, facilitating a more stable and potentially faster convergence. Here, we use a general way of updating each element of the step size matrices $\mathbf{\Phi}_{\mathbf{W}}^l$, $\mathbf{\Phi}_{\mathbf{F}_k}^l$, and $\mathbf{\Phi}_{\bar{\mathbf{F}}_k}^l$. Using a unified notation $\mathbf{\Phi}$ for any of these matrices, the update rule for the (i, j)th element can be written as

$$[\mathbf{\Phi}^{l+1}]_{i,j} = \frac{[\mathbf{\Phi}^l]_{i,j}}{\sqrt{[\mathbf{G}^l]_{i,j} + \zeta}}\ \forall i, j \tag{20}$$

where ζ is a small positive scalar added to avoid division by zero, and the element $[\mathbf{G}^l]_{i,j}$ records the sum of squared partial derivative for each element (ith row and jth column) of the corresponding variables accumulated over iterations. By implementing (20), we can dynamically adjusting the step size for individual elements of each variable.

In the next step, the Lagrange multiplier λ_k and penalty parameter ρ are updated as

$$\lambda_k^{l+1} = \lambda_k^l + \rho\Big(\|\mathbf{F}_k^l\|_F^2 + \|\bar{\mathbf{F}}_k^l\|_F^2 - P_{\max}\Big)\ \forall k \tag{21}$$

$$\rho^{l+1} = \begin{cases}\min(\xi\rho^l, \rho_{\max}), & \delta^l \geq \delta_{\text{th}}\\ \max(\frac{\rho^l}{\xi}, \rho_{\min}), & \delta^l < \delta'_{\text{th}}\\ \rho^l, & \text{otherwise}\end{cases} \tag{22}$$

where δ^l indicates the constraint violation between $\|\mathbf{F}_k^l\|_F^2 + \|\bar{\mathbf{F}}_k^l\|_F^2$ and $P_{\max}$, ξ is a scaling factor (e.g., 2) and $\rho_{\max}$ is a maximum value for ρ^{l+1} to prevent it from growing too large. In particular, ρ^{l+1} will be increased if the violation is significant, i.e., $\delta^l \geq \delta_{\text{th}}$; otherwise, ρ^{l+1} will be decreased if the violation δ^l is minor, i.e., $\delta^l < \delta'_{\text{th}}$. A minimum constraint $\rho_{\min}$ is considered to prevent ρ^{l+1} from becoming too small.

The GDAL algorithm is stopped once the bias of the value of the Lagrangian function is not greater than the tolerance ϵ or the maximum number of iterations L is reached. The detailed procedures of the GDAL algorithm are summarized in Algorithm 1. Thus, the optimal sensing precoder matrix $\mathbf{F}_k^*$ for each robot is derived, which will be used for the precoder and combiner design to achieve a performance tradeoff optimization in the next section.

$$\mathcal{L}_{P1.2}(\mathbf{F}_k, \mathbf{W}, \bar{\mathbf{F}}_k, \lambda_k, \rho) = \mathcal{F}_{1.2}\big(\mathbf{F}_k, \mathbf{W}, \bar{\mathbf{F}}_k\big) + \sum_{k=1}^{K}\lambda_k\Big(\|\mathbf{F}_k\|_F^2 + \|\bar{\mathbf{F}}_k\|_F^2 - P_{\max}\Big) + \frac{\rho}{2}\sum_{k=1}^{K}\Big(\|\mathbf{F}_k\|_F^2 + \|\bar{\mathbf{F}}_k\|_F^2 - P_{\max}\Big)^2 \tag{13}$$

B. Directional Beampattern Design

For the directional radar beampattern design, the directions of interest are specified in advance to design the covariance matrix $\mathbf{R}_k = \mathbf{F}_k\mathbf{F}_k^H \in \mathbb{C}^{N_t \times N_t}$ (Hermitian positive-definite matrix). Given the angle directions of interest, the covariance matrix $\mathbf{R}_k$ design can refer to the procedures stated in [43], [44]

$$\min_{\mathbf{F}_k} \quad \left|\mathbf{g}(\theta) - \mathbf{a}(\theta)^H\mathbf{F}_k\mathbf{F}_k^H\mathbf{a}(\theta)\right| \tag{23a}$$

$$\text{s.t.} \quad \|\mathbf{F}_k\|_F^2 = P_t \, \forall k \tag{23b}$$

where $\mathbf{a}(\theta) \in \mathbb{C}^{N_t \times 1}$ represents the steering vector in the direction of $\theta \in [-\pi/2, \pi/2]$ at the ULA of N_t transmitting antenna elements [33], $\mathbf{g}(\theta)$ denotes the desired beampattern [43], and $P_t \leq P_{\max}$ is the transmit power for radar sensing.[4]

Similar to the omnidirectional beampattern design, the MSE minimization problems about AirComp can be formulated as

$$\begin{aligned} \mathbf{P3.1} \quad \min_{\mathbf{F},\mathbf{W}} \quad & \mathcal{F}_{3.1}(\mathbf{F}_k, \mathbf{W}) \\ & = \sum_{k=1}^{K} \|\mathbf{W}^H\mathbf{H}_k\mathbf{F}_k - \mathbf{A}\|_F^2 + \sigma_n^2\|\mathbf{W}\|_F^2 && (24a) \\ \text{s.t.} \quad & \mathbf{F}_k\mathbf{F}_k^H = \mathbf{R}_k \, \forall k && (24b) \end{aligned}$$

and

$$\begin{aligned} \mathbf{P4.1} \quad \min_{\mathbf{F},\mathbf{W},\bar{\mathbf{F}}} \quad & \mathcal{F}_{4.1}\left(\mathbf{F}_k, \mathbf{W}, \bar{\mathbf{F}}_k\right) \\ & = \sum_{k=1}^{K} \|\mathbf{W}^H\mathbf{H}_k\mathbf{F}_k - \mathbf{A}\|_F^2 \\ & \quad + \sum_{k=1}^{K} \|\mathbf{W}^H\bar{\mathbf{H}}_k\bar{\mathbf{F}}_k\|_F^2 + \sigma_n^2\|\mathbf{W}\|_F^2 && (25a) \\ \text{s.t.} \quad & \bar{\mathbf{F}}_k\bar{\mathbf{F}}_k^H = \mathbf{R}_k \forall k, && (25b) \\ & \|\mathbf{F}_k\|_F^2 + \|\bar{\mathbf{F}}_k\|_F^2 = P_{\max} \, \forall k && (25c) \end{aligned}$$

for shared antenna configuration setup and separated antenna setup, respectively.

Similar to problems **P1.1** and **P2.1**, both **P3.1** and **P4.1** are nonconvex, and they can also be solved by the proposed GDAL algorithm presented in Algorithm 1. First, we define the augmented Lagrangian functions for **P3.1** and **P4.1** in (26) and (27), respectively, shown at the bottom of the page. Then, the problems can be solved by following the similar procedures described in Algorithm 1.[5]

Algorithm 1: GDAL Algorithm for Problem **P2.1**

Input: Initialize $\mathbf{W}^0$, $\mathbf{F}^0$, $\bar{\mathbf{F}}^0$, λ^0, ρ^0, tolerance ϵ, step sizes $\mathbf{\Phi}_{\mathbf{F}_k}^0$, $\mathbf{\Phi}_{\mathbf{W}}^0$ and $\mathbf{\Phi}_{\bar{\mathbf{F}}_k}^0$, maximum number of iterations L.

Output: Optimal $\mathbf{F}$, $\mathbf{W}$ and $\bar{\mathbf{F}}$

$l \leftarrow 0$;
while $l < L$ **do**
  Sequentially update the parameters:
  Compute the value of the Lagrangian function in (13);
  Compute gradients of augmented Lagrangian function with respect to $\bar{\mathbf{F}}_k$, $\mathbf{F}_k$ and $\mathbf{W}$ defined in (14)-(16);
  Update $\bar{\mathbf{F}}_k$, $\mathbf{F}_k$ and $\mathbf{W}$ using gradient descent approach according to (17)–(19);
  Adaptively update the step sizes according to (20);
  Update λ_k^{l+1} according to (21);
  Update ρ^{l+1} defined in (22);
  Check convergence criteria:
  if *convergence criteria met* **then**
    Output F, W and $\bar{\mathbf{F}}$;
    break;
  $l \leftarrow l + 1$;

IV. Beamforming Design for Performance Tradeoff Optimization

In addition to the shared and separated antenna configurations presented in Section II, two beampatterns (omnidirectional and directional) for sensing are also considered here. Therefore, there are four different combinations of beampattern schemes, as suggested by the optimal beampattern design problems of **P1.1–P4.1**, which are formulated in Section III. In this section, we consider the performance tradeoff optimization problems between AirComp and sensing given a weighting factor $\alpha \in [0, 1]$ and the optimal beampatterns $\mathbf{F}^* = \{\mathbf{F}_1^*, \ldots, \mathbf{F}_K^*\}$ that obtained from **P1.1–P4.1**. For a large α, the optimization efforts are directed toward minimizing the AirComp MSE, potentially at the expense of sensing accuracy. Conversely, for a small α, there is more emphasis

[4] This problem can be easily solved using the cvx toolbox [45], [46], more detailed discussion is out of the scope of this article.

[5] The detailed procedures are not presented again for the sake of brevity, as they follow the same steps.

$$\mathcal{L}_{P2.1}(\mathbf{F}_k, \mathbf{W}, \lambda_k, \rho) = \mathcal{F}_{2.1}(\mathbf{F}_k, \mathbf{W}) + \sum_{k=1}^{K} \lambda_k \mathbf{Tr}\left(\mathbf{F}_k\mathbf{F}_k^H - \mathbf{R}_k\right) + \frac{\rho}{2}\sum_{k=1}^{K}\|\mathbf{F}_k\mathbf{F}_k^H - \mathbf{R}_k\|_F^2 \tag{26}$$

$$\begin{aligned} \mathcal{L}_{P2.2}(\mathbf{F}_k, \mathbf{W}, \bar{\mathbf{F}}_k, \lambda_k^1, \lambda_k^2, \rho_1, \rho_2) = {} & \mathcal{F}_{2.2}\left(\mathbf{F}_k, \mathbf{W}, \bar{\mathbf{F}}_k\right) + \sum_{k=1}^{K} \lambda_k^1 \mathbf{Tr}\left(\bar{\mathbf{F}}_k\bar{\mathbf{F}}_k^H - \mathbf{R}_k\right) + \frac{\rho_1}{2}\sum_{k=1}^{K}\|\bar{\mathbf{F}}_k\bar{\mathbf{F}}_k^H - \mathbf{R}_k\|_F^2 \\ & + \sum_{k=1}^{K} \lambda_k^2\left(\|\mathbf{F}_k\|_F^2 + \|\bar{\mathbf{F}}_k\|_F^2 - P_{\max}\right) + \frac{\rho_2}{2}\sum_{k=1}^{K}\left(\|\mathbf{F}_k\|_F^2 + \|\bar{\mathbf{F}}_k\|_F^2 - P_{\max}\right)^2 \end{aligned} \tag{27}$$

on minimizing the sensing MSE, which improves sensing accuracy but may potentially decrease AirComp performance. In the case of cooperative communications and sensing, such as the use of dual-functional waveform for both sensing and communication that is sent by the same antenna, increasing α may not significantly affect the sensing MSE, especially when resources (e.g., transmit power) are abundant. However, in the competitive relationship between sensing and communication for resource allocation, an increase in α (i.e., more emphasis on communication for AirComp) might result in decreased sensing performance, especially when using separated antenna configurations for sensing and communication. Moreover, a lower sensing MSE is expected to be achieved with a directional beampattern compared to an omnidirectional one for a given antenna setup.

A. Problem Formulation With Performance Tradeoff Optimization

After deriving the optimal beamformer $\mathbf{F}_k^*$ for each robot $\forall k$, the performance tradeoff optimization problems for all robots, by considering the total power constraint and sensing QoS requirement, can be reformulated as

$$\mathbf{P1.2} \quad \min_{\mathbf{F},\mathbf{W}} \quad \alpha\mathcal{F}_{1.1}(\mathbf{F}_k, \mathbf{W}) + (1-\alpha)\sum_{k=1}^{K}\|\mathbf{F}_k - \mathbf{F}_k^*\|_F^2 \tag{28a}$$

$$\text{s.t.} \quad \|\mathbf{F}_k\|_F^2 \le P_{\max}\ \forall k, \tag{28b}$$

$$\|\mathbf{F}_k\|_F^{-2} \le \frac{\beta}{N_r\sigma_n^2}\ \forall k \tag{28c}$$

where the second term is weighted by $(1-\alpha)$ in (28a), and it represents the sensing performance loss. The constraint in (28c) indicates the sensing QoS requirement with a threshold β [32]. This tradeoff optimization problem corresponds to the one formulated in **P1.1** with the shared antenna structure and omnidirectional beampattern (denoted as the "*shared-omni*" scheme). For the other combinations of schemes, in terms of separated antenna structure with omnidirectional beampattern (denoted as "*separated-omni*" scheme), shared antenna structure with directional beampattern (denoted as "*shared-direction*" scheme), and separated antenna structure with directional beampattern (denoted as "*separated-direction*" scheme), the tradeoff optimization problems can be represented, respectively, as

$$\mathbf{P2.2} \quad \min_{\mathbf{F},\mathbf{W},\bar{\mathbf{F}}} \quad \alpha\mathcal{F}_{2.1}(\mathbf{F}_k, \mathbf{W}, \bar{\mathbf{F}}_k) + (1-\alpha)\sum_{k=1}^{K}\|\bar{\mathbf{F}}_k - \bar{\mathbf{F}}_k^*\|_F^2 \tag{29a}$$

$$\text{s.t.} \quad \|\mathbf{F}_k\|_F^2 + \|\bar{\mathbf{F}}_k\|_F^2 \le P_{\max}\ \forall k, \tag{29b}$$

$$\|\bar{\mathbf{F}}_k\|_F^{-2} \le \frac{\beta}{N_r\sigma_n^2}\ \forall k \tag{29c}$$

and

$$\mathbf{P3.2} \quad \min_{\mathbf{F},\mathbf{W}} \quad \alpha\mathcal{F}_{3.1}(\mathbf{F}_k, \mathbf{W}) + (1-\alpha)\sum_{k=1}^{K}\|\mathbf{F}_k - \mathbf{F}_k^*\|_F^2 \tag{30a}$$

$$\text{s.t.} \quad \text{(28b) and (28c)} \tag{30b}$$

and

$$\mathbf{P4.2} \quad \min_{\mathbf{F},\mathbf{W},\bar{\mathbf{F}}} \quad \alpha\mathcal{F}_{4.1}(\mathbf{F}_k, \mathbf{W}, \bar{\mathbf{F}}_k) + (1-\alpha)\sum_{k=1}^{K}\|\bar{\mathbf{F}}_k - \bar{\mathbf{F}}_k^*\|_F^2 \tag{31a}$$

$$\text{s.t.} \quad \text{(29b) and (29c)} \tag{31b}$$

which are corresponding to the beampattern design schemes in problems **P2.1**, **P3.1**, and **P4.1**, respectively.

B. Gradient Descent Augmented Lagrangian Method

Similar to the optimization problems **P1.1–P1.4**, we use the proposed GDAL algorithm to derive the desired $\mathbf{F}$, $\mathbf{W}$, and $\bar{\mathbf{F}}$. To demonstrate the procedures, we only select a more complex problem, i.e., problem **P4.2** for the scheme of "*separated-direction*," and show the detailed derivation only for this problem. The corresponding derivations for **P1.2−P3.2** follow similar procedures, which are not covered here for the sake of brevity.

First, the augmented Lagrangian function is defined in (32), shown at the bottom of the page, taking into account the maximum transmit power $P_{\max}$ and their sensing QoS requirement β. Before updating the variables $\mathbf{F}_k^l$, $\mathbf{W}^l$, and $\bar{\mathbf{F}}_k^l$ at the lth iteration using the gradient descent method, the corresponding gradients are computed as

$$\begin{aligned}
\nabla_{\mathbf{W}}\mathcal{L}_{P4.2} =&\ 2\alpha\sum_{k=1}^{K}\mathbf{H}_k\mathbf{F}_k\big(\mathbf{W}^H\mathbf{H}_k\mathbf{F}_k - \mathbf{A}\big)\\
&+2\alpha\left[\sum_{k=1}^{K}\bar{\mathbf{H}}_k^H\bar{\mathbf{F}}_k\mathbf{W}^H\bar{\mathbf{H}}_k\bar{\mathbf{F}}_k + 2\sigma_n^2\mathbf{W}\right]
\end{aligned}\tag{33}$$

$$\begin{aligned}
\nabla_{\mathbf{F}_k}\mathcal{L}_{P4.2} =&\ 2\alpha\mathbf{H}_k^H\mathbf{W}\big(\mathbf{W}^H\mathbf{H}_k\mathbf{F}_k - \mathbf{A}\big) + 2\lambda_k^1\mathbf{F}_k\\
&+2\rho_1\Big(\|\mathbf{F}_k\|_F^2 + \|\bar{\mathbf{F}}_k\|_F^2 - P_{\max}\Big)\ \forall k
\end{aligned}\tag{34}$$

$$\begin{aligned}
\nabla_{\bar{\mathbf{F}}_k}\mathcal{L}_{P4.2} =&\ 2\alpha\bar{\mathbf{H}}_k^H\mathbf{W}\mathbf{W}^H\bar{\mathbf{H}}_k\bar{\mathbf{F}}_k + 2(1-\alpha)\big(\bar{\mathbf{F}}_k - \bar{\mathbf{F}}_k^*\big)\\
&+2\rho_1\Big(\|\mathbf{F}_k\|_F^2 + \|\bar{\mathbf{F}}_k\|_F^2 - P_{\max}\Big)\bar{\mathbf{F}}_k\\
&-2\rho_2\left(\|\mathbf{F}_k\|_F^{-2} - \frac{\beta}{N_r\sigma_n^2}\right)\frac{\bar{\mathbf{F}}_k}{\|\bar{\mathbf{F}}_k\|_F^4}\\
&+2\lambda_k^1\bar{\mathbf{F}}_k - 2\lambda_k^2\frac{\bar{\mathbf{F}}_k}{\|\bar{\mathbf{F}}_k\|_F^4}\ \forall k
\end{aligned}\tag{35}$$

$$\begin{aligned}
\mathcal{L}_{P4.2}(\mathbf{F}_k, \mathbf{W}, \bar{\mathbf{F}}_k, \lambda_k^1, \lambda_k^2, \rho_1, \rho_2) =&\ \alpha\mathcal{F}_{4.1}\big(\mathbf{F}_k, \mathbf{W}, \bar{\mathbf{F}}_k\big) + (1-\alpha)\sum_{k=1}^{K}\|\bar{\mathbf{F}}_k - \bar{\mathbf{F}}_k^*\|_F^2 + \sum_{k=1}^{K}\lambda_1\Big(\|\mathbf{F}_k\|_F^2 + \|\bar{\mathbf{F}}_k\|_F^2 - P_{\max}\Big)\\
&+\frac{\rho_1}{2}\sum_{k=1}^{K}\Big(\|\mathbf{F}_k\|_F^2 + \|\bar{\mathbf{F}}_k\|_F^2 - P_{\max}\Big)^2 + \sum_{k=1}^{K}\lambda_k^2\left(\|\mathbf{F}_k\|_F^{-2} - \frac{\beta}{N_r\sigma_n^2}\right)\\
&+\frac{\rho_2}{2}\sum_{k=1}^{K}\left(\|\mathbf{F}_k\|_F^{-2} - \frac{\beta}{N_r\sigma_n^2}\right)^2.
\end{aligned}\tag{32}$$

Algorithm 2: GDAL Algorithm for Problem **P4.2**

Input: Initialize $\mathbf{F}_k^0$, $\mathbf{W}^0$, $\bar{\mathbf{F}}_k^0$, λ_1^0, λ_2^0, ρ_1^0, ρ_2^0, $\mathbf{\Phi}_{\mathbf{F}_k}^0$, $\mathbf{\Phi}_{\mathbf{W}}^0$, $\mathbf{\Phi}_{\bar{\mathbf{F}}_k}^0$, tolerance ϵ, and maximum number of iterations L.
Output: Optimal $\mathbf{F}$, $\mathbf{W}$ and $\bar{\mathbf{F}}$

```
l ← 0 ;
while l < L do
    Sequentially update the parameters:
    Compute the Lagrangian function value in (32);
    Compute gradients of ∇_W L_P4.2, ∇_{F_k} L_P4.2 and ∇_{F̄_k} L_P4.2 according to (33)–(35);
    Update F_k^{l+1}, W^{l+1} and F̄_k^{l+1} according to (17)-(19);
    Update Lagrange multipliers (λ_k^1)^{l+1} and (λ_k^2)^{l+1} in (36)–(37);
    Update penalty parameter: ρ_1^{l+1} and ρ_2^{l+1} according to the rule defined in (22);
    Check convergence criteria:
    if convergence criteria met then
        Output F, W and F̄ ;
        break;
    l ← l + 1 ;
```

Then, these variables are updated according to the updating rules defined in (17)–(19). Note that we also implement the AdaGrad method to adaptively updating the step sizes $\mathbf{\Phi}_{\mathbf{W}}$, $\mathbf{\Phi}_{\mathbf{F}_k}$, and $\mathbf{\Phi}_{\bar{\mathbf{F}}_k}$ for fast convergence. The Lagrange multipliers λ_k^1 and λ_k^2 are sequentially updated as

$$(\lambda_k^1)^{l+1} = (\lambda_k^1)^l + \rho_1^l\left(\|\mathbf{F}_k^{l+1}\|_F^2 + \|\bar{\mathbf{F}}_k^{l+1}\|_F^2 - P_{\max}\right)\forall k \quad (36)$$

$$(\lambda_k^2)^{l+1} = (\lambda_k^2)^l + \rho_2^l\left(\|\bar{\mathbf{F}}_k^{l+1}\|_F^{-2} - \frac{\beta}{N_r\sigma_n^2}\right)\forall k. \quad (37)$$

Corresponding updates of ρ_1 and ρ_2 follow the rule specified in (22). The overall algorithm stops once the bias of the value of the Lagrangian function is not greater than the tolerance ϵ or the maximum number of iterations L is reached. Finally, we obtain $\mathbf{F}_k$, $\mathbf{W}$, and $\bar{\mathbf{F}}_k$ for sensing and AirComp under the constraints. The detailed derivation procedures are summarized in Algorithm 2.

C. Complexity Analysis

By implementing adaptive adjustments of the step size in the gradient descent-based algorithm, the number of iterations for convergence can potentially be reduced, as stated in [47]. In this section, we analyze the worst case computational complexity of Algorithm 1 for solving problem **P4.2**.[6] At each iteration l, the computational complexity is dominated by the matrix multiplications required for calculating the gradients when updating the variables (i.e., $\mathbf{W}$, $\mathbf{F}_k$, and $\bar{\mathbf{F}}_k$). The related computational complexities are $\mathcal{O}(KMN_AN_t + MN_A)$, $\mathcal{O}(KMN_AN_c)$, and $\mathcal{O}(KMN_AN_s)$, respectively. Therefore, the worst case computational complexity with L iterations using our GDAL algorithm for solving problem **P4.2** is $\mathcal{O}(LKMN_AN_t+LMN_A)$, where $N_t = N_c+N_s$ as defined in Section II-B. It is observed that the computational complexity is proportional to the number of cooperative robots. However, a certain number of robots is expected to be sufficient to meet the QoS requirements in terms of sensing and AirComp via uplink communications, which will be verified in the next section. In this case, our scheme is scalable to an IoRT scenario with a large number of robots because we only need to select a subset of robots covered by the AP. Moreover, our analysis is more practical as it considers the path loss and blockage effects.

[6] The computational analysis for solving **P1.2–P3.2** follows a similar procedure and is not presented here.

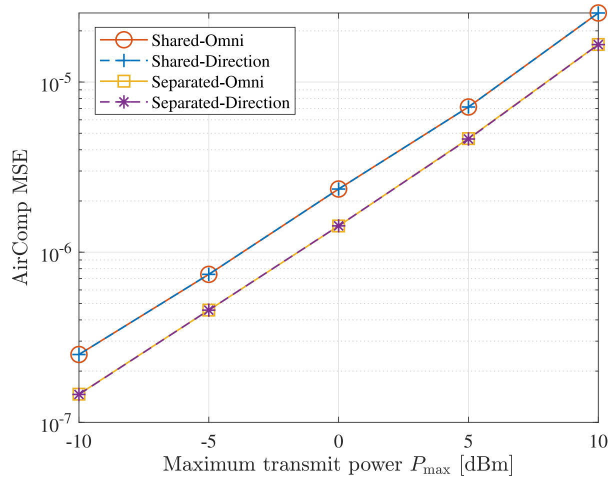

Fig. 2. AirComp MSE under different levels of power constraint: $K = 10, p_b = 0$.

V. Numerical Simulation

For comprehensive comparisons among the different combinations of antenna structures and beampattern types, the performance evaluation using our proposed algorithms is presented in this section. We assume that the AP has $N_A = 32$ antenna elements, and each robot has a total of $N_R = 24$ antenna elements. In the shared antenna structure setup, $N_t = N_r = 12$ for signal transmission and reception. For a fair comparison, we use the same number of antenna elements at each robot in the separated antenna structure setup, e.g., $N_s = N_c = 8$ for sensing and communication, and $N_r = 8$ for signal reception at the robot. For the IoRT scenario depicted in Fig. 1, the link condition between each robot and AP is modeled as follows: the link is assumed to be blocked with a probability p_b, and path loss is calculated following the 3GPP [35]. We assume that the robot–AP link condition is either in LoS or Non-LoS (NLoS) with a dominant single path propagation, i.e., $M = 1$. However, we can extend it to any integer M according to the practical channel conditions to support the case of $M > 1$ AirComp functions. Furthermore, we use the abbreviation terms "*shared-omni*," "*shared-direction*," "*separated-omni*," and "*separated-direction*" to distinguish between different antenna and beampattern setups. The performance tradeoff between AirComp and sensing is weighted by a factor $\alpha = 0.5$ if no other specifications are given.

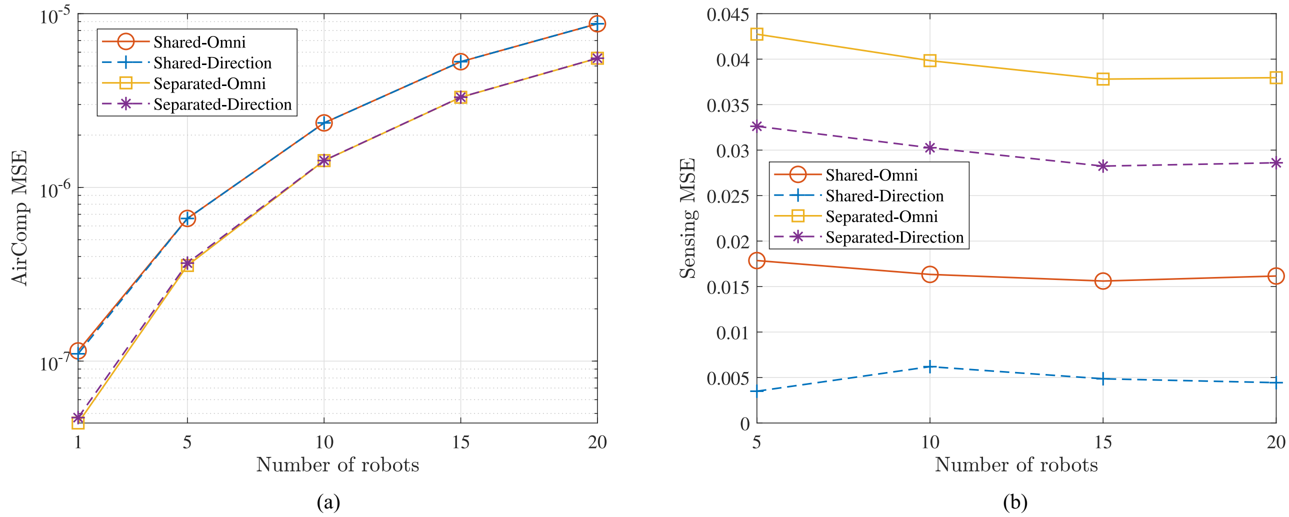

Fig. 3. MSE performance affected by the number of robots ($P_{\max} = 0$ dBm, $p_b = 0$): (a) AirComp MSE and (b) sensing MSE.

Fig. 2 illustrates the AirComp MSE under different maximum transmit power budgets. The AirComp MSE increases with the maximum power $P_{\max}$. Moreover, the MSE is in the range of approximately 10^{-7} to 10^{-5}. Those phenomena are due to the path loss, which results in a low received power level. It is meaningful for practical deployment, which is different from the case of simple Gaussian channel modeling with zero mean and unit variance, as considered in [6] and [32]. It is also interesting to observe that beampattern types (omnidirectional and directional) almost have no effect on the AirComp MSE for the given antenna structure (shared or separated). This is because the AP itself can realize a variable beamwidth to cover all the robots within its sector area for uplink aggregated signal reception [33]. In such a case, the optimal beamforming combiner at the AP can be guaranteed. Moreover, one of our objectives is to minimize the AirComp MSE so that the expected beamforming precoder at each robot can also be ensured compared to the optimal one using our algorithm. Compared to the shared antenna setup, the AirComp MSE of the separated antenna configuration can be reduced by approximately 40%, even as the number of robots increases. This verifies that the separated antenna array for communication and sensing achieves a higher degree of freedom for beam steering compared to the dual-functional beamforming in a shared antenna structure.

If the number of robots increases, it is challenging to design an aggregation beamforming combiner at the AP to receive the uplink AirComp signals within its coverage. This is because the larger the number of robots randomly distributed within the AP's coverage area, the larger the beamwidth is needed for the AP to cover all the robots, which results in a lower beamforming gain such that a larger MSE is obtained, as shown in Fig. 3(a) at the top of the page. In addition, the separated antenna structure has a lower AirComp MSE than the shared antenna structure, which is similar to the results shown in Fig. 2. This is because it has a higher degree of freedom for spatial beam steering. Moreover, the beampattern has almost no effect on the MSE for a given antenna structure. Fig. 3(b) shows that the sensing MSE maintains a relatively stable level for given setups though a slightly decrease for the separated antenna configurations. It is due to the sensing precoder is derived for each robot separately so that the sensing performance can always be guaranteed, and it is almost not affected by the number of robots. The increased number of robots only has significant effects on aggregation beamforming design at the AP, which reflects in the AirComp performance, as illustrated in Fig. 3(a). Therefore, the expected average system performance in terms of AirComp and sensing can be achieved by selecting a subset of cooperative robots covered by the AP, rather than using the information from all robots. This approach helps to reduce the computational complexity of implementing our proposed algorithm in practice, as stated in Section IV-C. Furthermore, it is observed that the directional beampattern achieves a lower sensing MSE for a given antenna structure setup. The separated antenna structure configuration yields a higher sensing MSE than the shared antenna setup because the separated antenna setup has an enhanced DoF for sensing beam steering but with a decreased transmit power.

The performance analysis above assumes a fair tradeoff factor between sensing and AirComp, i.e., $\alpha = 0.5$. The weight of the sensing MSE decreases with increasing α. In addition, the order of magnitude of the sensing MSE (i.e., beampattern) is larger than that of AirComp due to the path-loss effect, as illustrated in Fig. 3. This results in a notable decrease in the value of Lagrangian function with increasing α, as depicted in Fig. 4. Moreover, the directional beampattern achieves a lower value of the Lagrangian function compared to the omnidirectional one for the given antenna setup and α. Particularly, the optimization problems convert to the ones of only minimizing the AirComp MSE when $\alpha = 1$.

We also evaluate the blockage probability effects on the AirComp MSE in Fig. 5. The blockage probability has remarkable effects on the scheme of the separated antenna structure compared to the shared antenna setup. This is due to the fact that the separated antenna configuration has a power division into two antenna arrays for sensing and AirComp, respectively.

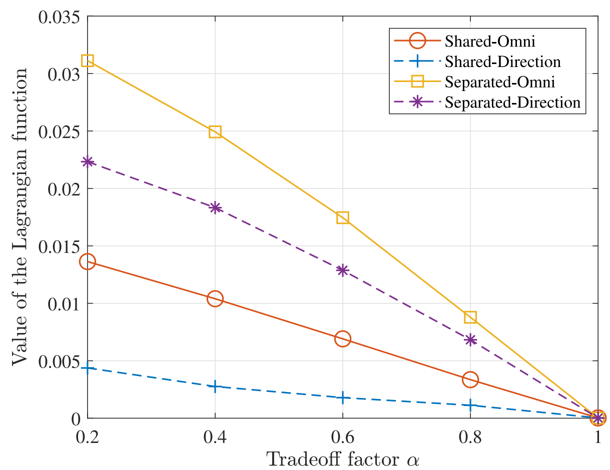

Fig. 4. Tradeoff factor effects on the value of the Lagrangian function: $K = 10, P_{\max} = 10\,\mathrm{dBm}, p_b = 0$.

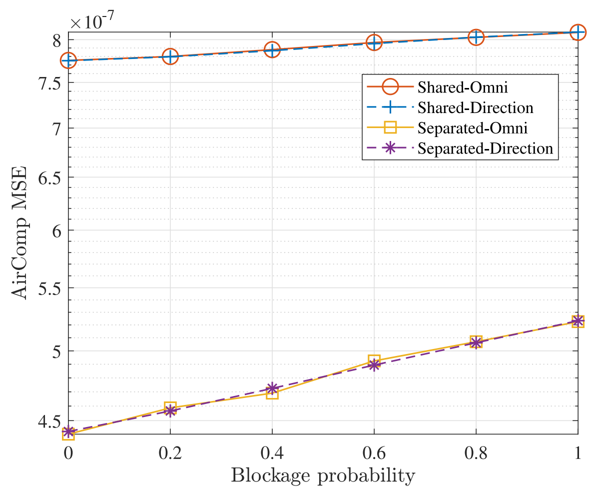

Fig. 5. Blockage effects on the AirComp MSE: $K = 5, P_{\max} = 0\,\mathrm{dBm}$.

This causes uplink AirComp to have low transmit power. Furthermore, the AirComp link between each robot and the AP is not fully blocked even if a blockage event occurs [35], [48]. As a consequence, the AirComp MSE for the shared antenna setup does not show a remarkably sharp increase with the blockage probability.

VI. Conclusion

In this article, a comprehensive investigation of the antenna structures and beampatterns for the ISCC system in an IoRT scenario has been presented. There are four MSE minimization optimization problems formulated among different setups in terms of "*shared-omni*," "*shared-direction*," "*separated-omni*," and "*separated-direction*" that involve a weighted factor to tradeoff the performance between AirComp and sensing. To efficiently solve the formulated nonconvex optimization problems, we have designed the GDAL algorithm with an adaptive adjustment of the step sizes in the variable updates. The simulations have shown that the separated antenna structure achieves a lower AirComp MSE than the shared antenna setups because it has higher DoF for beam steering. Moreover, the beampattern has almost no effect on the AirComp MSE for a given antenna structure setup at the robots. The required system performance in terms of AirComp MSE and sensing MSE can be achieved by selecting only a subset of cooperative robots rather than using all the robots within the AP's coverage. This scalability allows our proposed scheme to be applicable to an IoRT scenario with a large number of robots. Therefore, we must strike a balance between complexity and target localization accuracy in practical IoRT scenarios. Moreover, it is more sensitive to the blockage for the separated antenna setups due to the power split for sensing and communication, which results in a remarkable increase in AirComp MSE as the blockage probability increases. These findings have meaningful guidelines for practical IoRT networks. For instance, leveraging our proposed scheme for accurate target localization, we can select appropriate radio propagation paths to mitigate blockages, ensuring timely packet delivery within specified low-latency constraints in deterministic wireless networking.

Acknowledgment

This article reflects only the authors' views, and the European Commission bears no responsibility for any utilization of the information contained herein.

References

[1] D. C. Nguyen et al., "6G Internet of Things: A comprehensive survey," *IEEE Internet Things J.*, vol. 9, no. 1, pp. 359–383, Jan. 2022.

[2] Y. Liu et al., "Robotic communications for 5G and beyond: Challenges and research opportunities," *IEEE Commun. Mag.*, vol. 59, no. 10, pp. 92–98, Oct. 2021.

[3] 4 F. Liu et al., "Integrated sensing and communications: Toward dual-functional wireless networks for 6G and beyond," *IEEE J. Sel. Areas Commun.*, vol. 40, no. 6, pp. 1728–1767, Jun. 2022.

[4] Y. Cui, F. Liu, X. Jing, and J. Mu, "Integrating sensing and communications for ubiquitous IoT: Applications, trends, and challenges," *IEEE Netw.*, vol. 35, no. 5, pp. 158–167, Sep./Oct. 2021.

[5] S. H. Alsamhi, O. Ma, and M. S. Ansari, "Survey on artificial intelligence based techniques for emerging robotic communication," *Telecommun. Syst.*, vol. 72, pp. 483–503, Mar. 2019.

[6] X. Li et al., "Integrated sensing, communication, and computation over-the-air: MIMO beamforming design," *IEEE Trans. Wireless Commun.*, vol. 22, no. 8, pp. 5383–5398, Aug. 2023.

[7] A. Liu et al., "A survey on fundamental limits of integrated sensing and communication," *IEEE Commun. Surveys Tuts.*, vol. 24, no. 2, pp. 994–1034, 2nd Quart., 2022.

[8] F. Liu and C. Masouros, "A tutorial on joint radar and communication transmission for vehicular networks—Part I: Background and fundamentals," *IEEE Commun. Lett.*, vol. 25, no. 2, pp. 322–326, Feb. 2021.

[9] A. Hassanien, M. G. Amin, Y. D. Zhang, and F. Ahmad, "Dual-function radar-communications: Information embedding using sidelobe control and waveform diversity," *IEEE Trans. Signal Process.*, vol. 64, no. 8, pp. 2168–2181, Apr. 2016.

[10] K. V. Mishra, B. Shankar, V. Koivunen, B. Ottersten, and S. A. Vorobyov, "Toward millimeter-wave joint radar communications: A signal processing perspective," *IEEE Signal Process. Mag.*, vol. 36, no. 5, pp. 100–114, Sep. 2019.

[11] F. Liu, L. Zhou, C. Masouros, A. Li, W. Luo, and A. Petropulu, "Toward dual-functional radar-communication systems: Optimal waveform design," *IEEE Trans. Signal Process.*, vol. 66, no. 16, pp. 4264–4279, Aug. 2018.

[12] P. Kumari, S. A. Vorobyov, and R. W. Heath, "Adaptive virtual waveform design for millimeter-wave joint communication–radar," *IEEE Trans. Signal Process.*, vol. 68, pp. 715–730, Nov. 2019.

[13] Z. Xiao and Y. Zeng, "Full-duplex integrated sensing and communication: Waveform design and performance analysis," in *Proc. IEEE 13th Int. Conf. Wireless Commun. Signal Process. (WCSP)*, Changsha, China, 2021, pp. 1–5.

[14] Z. Wei et al., "Waveform design for MIMO-OFDM integrated sensing and communication system: An information theoretical approach," *IEEE Trans. Commun.*, vol. 72, no. 1, pp. 496–509, Jan. 2024.

[15] Z. Xing, R. Wang, and X. Yuan, "Joint active and passive beamforming design for reconfigurable intelligent surface enabled integrated sensing and communication," *IEEE Trans. Commun.*, vol. 71, no. 4, pp. 2457–2474, Apr. 2023.

[16] X. Liu, Y. Liu, Z. Liu, and T. S. Durrani, "Fair integrated sensing and communication for multi-UAV enabled Internet of Things: Joint 3D trajectory and resource optimization," *IEEE Internet Things J.*, early access, Oct. 25, 2023, doi: 10.1109/JIOT.2023.3327445.

[17] X. Li, Y. Gong, K. Huang, and Z. Niu, "Over-the-air integrated sensing, communication, and computation in IoT networks," *IEEE Wireless Commun.*, vol. 30, no. 1, pp. 32–38, Feb. 2023.

[18] P. Porambage, J. Okwuibe, M. Liyanage, M. Ylianttila, and T. Taleb, "Survey on multi-access edge computing for Internet of Things realization," *IEEE Commun. Surveys Tuts.*, vol. 20, no. 4, pp. 2961–2991, 4th Quart., 2018.

[19] T. Taleb, K. Samdanis, B. Mada, H. Flinck, S. Dutta, and D. Sabella, "On multi-access edge computing: A survey of the emerging 5G network edge cloud architecture and orchestration," *IEEE Commun. Surveys Tuts.*, vol. 19, no. 3, pp. 1657–1681, 3rd Quart., 2017.

[20] Y. Chen, N. Zhang, Y. Zhang, and X. Chen, "Dynamic computation offloading in edge computing for Internet of Things," *IEEE Internet Things J.*, vol. 6, no. 3, pp. 4242–4251, Jun. 2019.

[21] Q. Wang, R. Q. Hu, and Y. Qian, "Hierarchical energy-efficient mobile-edge computing in IoT networks," *IEEE Internet Things J.*, vol. 7, no. 12, pp. 11626–11639, Dec. 2020.

[22] W. Fan et al., "Joint task offloading and resource allocation for vehicular edge computing based on V2I and V2V modes," *IEEE Trans. Intell. Transp. Syst.*, vol. 24, no. 4, pp. 4277–4292, Apr. 2023.

[23] Y. Liao et al., "Low-latency data computation of inland waterway USVs for RIS-assisted UAV MEC network," *IEEE Internet Things J.*, early access, Apr. 15, 2024, doi: 10.1109/JIOT.2024.3387017.

[24] Z. Zhuang, D. Wen, Y. Shi, G. Zhu, S. Wu, and D. Niyato, "Integrated sensing-communication-computation for over-the-air edge AI inference," *IEEE Trans. Wireless Commun.*, vol. 23, no. 4, pp. 3205–3220, Apr. 2023.

[25] Q. Qi, X. Chen, C. Zhong, and Z. Zhang, "Integrated sensing, computation and communication in B5G cellular Internet of Things," *IEEE Trans. Wireless Commun.*, vol. 20, no. 1, pp. 332–344, Jan. 2021.

[26] G. Zhu, J. Xu, K. Huang, and S. Cui, "Over-the-air computing for wireless data aggregation in massive IoT," *IEEE Wireless Commun.*, vol. 28, no. 4, pp. 57–65, Aug. 2021.

[27] W. Fang, Y. Jiang, Y. Shi, Y. Zhou, W. Chen, and K. B. Letaief, "Over-the-air computation via reconfigurable intelligent surface," *IEEE Trans. Commun.*, vol. 69, no. 12, pp. 8612–8626, Dec. 2021.

[28] Z. Chen, E. G. Larsson, C. Fischione, M. Johansson, and Y. Malitsky, "Over-the-air computation for distributed systems: Something old and something new," *IEEE Netw.*, vol. 37, no. 5, pp. 240–246, Sep. 2023.

[29] A. Şahin and R. Yang, "A survey on over-the-air computation," *IEEE Commun. Surveys Tuts.*, vol. 25, no. 3, pp. 1877–1908, 3rd Quart., 2023.

[30] Q. Qi, X. Chen, A. Khalili, C. Zhong, Z. Zhang, and D. W. K. Ng, "Integrating sensing, computing, and communication in 6G wireless networks: Design and optimization," *IEEE Trans. Commun.*, vol. 70, no. 9, pp. 6212–6227, Sep. 2022.

[31] Y. Zuo, M. Yue, H. Yang, L. Wu, and X. Yuan, "Integrating communication, sensing and computing in satellite Internet of Things: Challenges and opportunities," *IEEE Wireless Commun.*, vol. 31, no. 3, pp. 332–338, Jun. 2024.

[32] S. Wang, Y. Gong, X. Li, and Q. Li, "Integrated sensing, communication, and computation over the air: Beampattern design for wireless sensor networks," *IEEE Internet Things J.*, vol. 11, no. 6, pp. 9681–9692, Mar. 2024.

[33] K. Dong, S. Mura, M. Mizmizi, D. Tagliaferri, and U. Spagnolini, "Advanced tri-sectoral multi-user millimeter-wave smart repeater," in *Proc. IEEE Int. Mediterr. Conf. Commun. Netw. (MeditCom)*, Dubrovnik, Croatia, 2023, pp. 205–210.

[34] Z. Liu, Y. Liu, and X. Chu, "Reconfigurable-intelligent-surface-assisted indoor millimeter-wave communications for mobile robots," *IEEE Internet Things J.*, vol. 11, no. 1, pp. 1548–1557, Jan. 2024.

[35] "Study on channel model for frequencies from 0.5 to 100 GHz," 3GPP, Sophia Antipolis, France, Rep. TR 38.901, Dec. 2019.

[36] A. Alkhateeb, O. El Ayach, G. Leus, and R. W. Heath, "Channel estimation and hybrid precoding for millimeter wave cellular systems," *IEEE J. Sel. Topics Signal Process.*, vol. 8, no. 5, pp. 831–846, Oct. 2014.

[37] A. Abdallah, A. Celik, M. M. Mansour, and A. M. Eltawil, "RIS-aided mmWave MIMO channel estimation using deep learning and compressive sensing," *IEEE Trans. Wireless Commun.*, vol. 22, no. 5, pp. 3503–3521, May 2023.

[38] A. M. Elbir, K. V. Mishra, S. A. Vorobyov, and R. W. Heath, "Twenty-five years of advances in beamforming: From convex and nonconvex optimization to learning techniques," *IEEE Signal Process. Mag.*, vol. 40, no. 4, pp. 118–131, Jun. 2023.

[39] Y. You, W. Zhao, L. Zhang, X. You, and C. Zhang, "Beam pattern and reflection pattern design for channel estimation in RIS-assisted Mmwave MIMO systems," *IEEE Trans. Veh. Technol.*, vol. 73, no. 4, pp. 5915–5919, Apr. 2024.

[40] D. P. Kingma and J. Ba, "Adam: A method for stochastic optimization," in *Proc. 3rd Int. Conf. Learn. Represent. (ICLR)*, San Diego, CA, USA, 2015, pp. 1–15.

[41] L. Luo, Y. Xiong, Y. Liu, and X. Sun, "Adaptive gradient methods with dynamic bound of learning rate," in *Proc. 3rd Int. Conf. Learn. Represent. (ICLR)*, New Orleans, LA, USA, 2019, pp. 1–19.

[42] J. Duchi, E. Hazan, and Y. Singer, "Adaptive subgradient methods for online learning and stochastic optimization," *J. Mach. Learn. Res.*, vol. 12, no. 7, pp. 2121–2159, 2011.

[43] A. Khabbazibasmenj, A. Hassanien, S. A. Vorobyov, and M. W. Morency, "Efficient transmit beamspace design for search-free based DOA estimation in MIMO radar," *IEEE Trans. Signal Process.*, vol. 62, no. 6, pp. 1490–1500, 2014.

[44] A. Hassanien and S. A. Vorobyov, "Phased-MIMO radar: A tradeoff between phased-array and MIMO radars," *IEEE Trans. Signal Process.*, vol. 58, no. 6, pp. 3137–3151, Jun. 2010.

[45] M. Grant and S. Boyd. "CVX: MATLAB software for disciplined convex programming, version 2.1." 2014. [Online]. Available: https://cvxr.com/cvx/

[46] M. C. Grant and S. P. Boyd, "Graph implementations for nonsmooth convex programs," in *Recent Advances Learning Control*. London, U.K.: Springer, 2008, pp. 95–110.

[47] S. H. Haji and A. M. Abdulazeez, "Comparison of optimization techniques based on gradient descent algorithm: A review," *PalArch's J. Archaeol. Egypt/Egyptol.*, vol. 18, no. 4, pp. 2715–2743, 2021.

[48] K. Dong, M. Mizmizi, D. Tagliaferri, and U. Spagnolini, "Vehicular blockage modelling and performance analysis for mmwave V2V communications," in *Proc. IEEE Int. Conf. Commun.*, Seoul, South Korea, 2022, pp. 3604–3609.

Kai Dong (Member, IEEE) received the Ph.D. degree in information technology from the Politecnico di Milano, Milan, Italy, in 2023.

He is currently a Postdoctoral Researcher with the Center of Wireless Communications, University of Oulu, Oulu, Finland, and a Visiting Researcher with the Department of Information and Communications Engineering, Aalto university, Espoo, Finland. His research interests include integrated sensing, computing, and communication, deterministic wireless communications, advanced relaying technologies in wireless, and optimization algorithms in signal processing.

Sergiy A. Vorobyov (Fellow, IEEE) received the M.Sc. and Ph.D. degrees in systems and control from the National University of Radio Electronics, Kharkiv, Ukraine, in 1994 and 1997, respectively.

He is a Professor with the Department of Information and Communications Engineering, Aalto University, Espoo, Finland. Since his graduation, he held various faculty and research positions with the University of Alberta, Edmonton, AB, Canada; the Joint Research Institute between Heriot–Watt University and Edinburgh University, U.K.; Duisburg–Essen University, Duisburg, Germany; Darmstadt University of Technology, Darmstadt, Germany; McMaster University, Hamilton, ON, Canada; the Institute of Physical and Chemical Research, Wako, Japan; and the National University of Radio Electronics. His research interests include optimization and multilinear algebra methods in signal processing and data analysis; statistical and array signal processing; sparse signal processing; computational imaging; estimation, detection, and learning theory and methods; and multiantenna, very large, cooperative, and cognitive systems.

Dr. Vorobyov is the recipient of the 2004 IEEE Signal Processing Society Best Paper Award, the 2007 Alberta Ingenuity New Faculty Award, the 2011 Carl Zeiss Award (Germany), the 2012 NSERC Discovery Accelerator Award, and the IEEE ICASSP 2023 Top 3% Paper Recognition. He has been the Senior Area Editor of the IEEE SIGNAL PROCESSING LETTERS since 2016. He was an Associate Editor of the IEEE TRANSACTIONS ON SIGNAL PROCESSING from 2006 to 2010 and the IEEE SIGNAL PROCESSING LETTERS from 2007 to 2009. He was a member of the Sensor Array and Multi-Channel Signal Processing and Signal Processing for Communications and Networking Technical Committees of the IEEE Signal Processing Society from 2007 to 2012 and from 2010 to 2016, respectively. He was the Track Chair of Asilomar 2011, Pacific Grove, CA, USA; the Technical Co-Chair of IEEE CAMSAP 2011, Puerto Rico; the Tutorial Chair of ISWCS 2013, Ilmenau, Germany; the Technical Co-Chair of IEEE SAM 2018, Sheffield, U.K.; the Technical Co-Chair of IEEE CAMSAP 2023, Costa Rica; and the General Co-Chair of EUSIPCO 2023, Helsinki, Finland.

Hao Yu (Member, IEEE) received the B.E. and Ph.D. degrees in communication engineering from Beijing University of Posts and Telecommunications, Beijing, China, in 2015 and 2020, respectively.

He was also a joint-supervised Ph.D. student with the Politecnico di Milano, Milan, Italy, and a Postdoctoral Researcher with the Center of Wireless Communications, University of Oulu, Oulu, Finland. He is currently a Senior Researcher with ICTFICIAL Oy, Espoo, Finland. His research interests include network automation, SDN/NFV, time-sensitive networks, and deterministic networking.

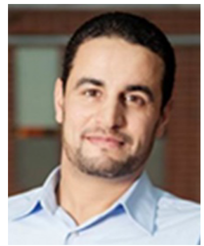

Tarik Taleb (Senior Member, IEEE) received the B.E. degree (with Distinction) in information engineering and the M.Sc. and Ph.D. degrees in information sciences from Tohoku University, Sendai, Japan, in 2001, 2003, and 2005, respectively.

He is currently a Full Professor with Ruhr University Bochum, Bochum, Germany. He was a Professor with the Center of Wireless Communications, University of Oulu, Oulu, Finland. He is the Founder of ICTFICIAL Oy, and the Founder and the Director of MOSA!C Lab, Espoo, Finland. From October 2014 to December 2021, he was an Associate Professor with the School of Electrical Engineering, Aalto University, Espoo. Prior to that, he was working as a Senior Researcher and a 3GPP Standards Expert with NEC Europe Ltd., Heidelberg, Germany. Before joining NEC and till March 2009, he worked as an Assistant Professor with the Graduate School of Information Sciences, Tohoku University, in a lab fully funded by KDDI. From 2005 to 2006, he was a Research Fellow with the Intelligent Cosmos Research Institute, Sendai. He has been directly engaged in the development and standardization of the Evolved Packet System as a member of the 3GPP System Architecture Working Group. His current research interests include AI-based network management, architectural enhancements to mobile core networks, network softwarization and slicing, mobile cloud networking, SDN/NFV, software-defined security, and mobile multimedia streaming.